# SOL-GEL COMBUSTION SYNTHESIS AND CHARACTERIZATION OF LiMn$_{1.95-x}$Co$_{0.05}$Cr$_X$O$_4$ CATHODE MATERIALS

**Paulos Taddesse Shibeshi[1]\*, Alemayehu Asefa[2]**

[1]*\*Assistant Professor, Department of Physics, College of Natural Science, Arba Minch University, Arba Minch, Ethiopia*
[2]*Gessa Secondary High School, Dawro Zone, Gena Bossa Wereda, Gessa, Ethiopia*

-----------------------------------------------------------------------***----------------------------------------------------------------------

**Abstract -** *LiMn$_{1.92}$Co$_{0.05}$Cr$_{0.03}$O$_4$ and LiMn$_{1.9}$Co$_{0.05}$Cr$_{0.05}$O$_4$ cathode materials are successfully synthesized by sol-gel combustion method, using citric acid as the starting materials. The structure of both cathode materials is characterized by x-ray diffraction (XRD) and Fourier transform infrared (FT-IR) spectroscopy. The electrical and dielectric properties are also investigated using impedance spectroscopy (IS). The XRD patterns reveal that the synthesized sample belongs to Fd3m space group with spinel structure. Moreover, both samples exhibit the same structure as pure LiMn$_2$O$_4$ spinel phase. It is also found that the dielectric constant, the real and imaginary parts of the impedance decrease with increase in frequency. From the frequency dependent plot of electrical conductivity, two different regions associated with different phenomena are identified. In the low frequency region, the conductivity is due to the electrode–electrolyte interface phenomena. In the high frequency region, the ionic conductivity increases with increasing frequency which is a characteristic of hopping process, indicating correlated forward–backward motion of charge carrier. The Nyquist plots of both compounds confirms the conductivity behavior of both samples is mixed electronic and ionic in character.*

*Keywords*: Cathode material, Sol-gel composition, Electrical property, Dielectric property.

## 1. INTRODUCTION

Cathode electrode is one of the key components in any type of batteries. More importantly, it affects the energy capacity, voltage, cycle life, safety and other basic properties of energy storage materials [1,2]. Thus, the characteristics of the materials used as the active cathodes are one of the decisive factors to affect the performance of a lithium-ion battery. The basic requirements for a material to be used as cathode in lithium-ion battery are as follows [3-4]: structurally stable for repeated charging/discharging processes, stable in contact with the electrolytes, adequate electronic and ionic conductivity, high potential, low cost, non-toxic (environmentally friendly), easily prepared, easily handled. However, all the existing cathode materials cannot meet all the above requirements at one time. Thus, research and development of new types of cathode materials with better electrochemical characteristics has been a hot topic in Li-ion battery research field.

For cathode electrode, there are different kinds of materials which have been widely studied and applied commercially, including lithium cobalt oxide LiCoO$_2$, lithium manganese oxide LiMn$_2$O$_4$, and lithium iron phosphate LiFePO$_4$. Among these cathode materials, LiCoO$_2$ is widely used in lithium ion technology. However, LiCoO$_2$ has some disadvantages such as high cost, not environmentally benign and low practical specific capacity against its theoretical value [5,6].

The spinel LiMn$_2$O$_4$ material belongs to Fd3m space group [7], and its structure consists of cubic close-packed oxygen ions in 32e sites, Li-ions in the 8a tetrahedral sites, and manganese ions in the 16d octahedral sites [8]. Furthermore, the spinel LiMn$_2$O$_4$ contains empty tetrahedral 8b and 48f, and octahedral 16c sites. In the spinel structure, the 8a tetrahedral sites are situated farthest from the 16d octahedra sites, and these two sites share each of their four faces with adjacent vacant 16c octahedra. This arrangement provides a three-dimensional pathway for Li-ion diffusion along the 8a–16c–8a path [7], or the diffusion process takes place from one 8a site to another 8a site through the intermediate 16c site. On the other hand, the electronic conductivity of LiMn$_2$O$_4$ is only 2×10$^{-5}$ - 5×10$^{-5}$ Scm$^{-1}$, which is much lower than that of LiCoO$_2$ ($\sim$10$^{-3}$ Scm$^{-1}$) [9,10].

Taking these aspects into account, we have successfully synthesized the new composition LiMn$_{1.92}$Co$_{0.05}$Cr$_{0.03}$O$_4$ and LiMn$_{1.9}$Co$_{0.05}$Cr$_{0.05}$O$_4$ cathode materials by sol–gel combustion method. In this paper, the results of structure, electrical and dielectric properties study of these samples are presented.

## 2. MATERIALS AND METHODS

### 2.1. Synthesis

Nanoparticles of LiMn$_{1.92}$Co$_{0.05}$Cr$_{0.03}$O$_4$ and LiMn$_{1.9}$Co$_{0.05}$Cr$_{0.05}$O cathode materials are prepared by using citrate gel combustion method. In this technique, oxidizing metal salts and combustion agent (fuel) are essential for the combustion process. Metal nitrates and citric acid are used as oxidizing salts and combustion fuel for both sample preparations. To synthesize both samples, LiNO$_3$, Mn(NO$_3$)$_3$. 6H$_2$O, Co(NO$_3$)$_3$. 6H$_2$O, Cr(NO$_3$)$_3$. 9H$_2$O and citric acid, C$_6$H$_8$O$_7$ are used as starting materials. The stoichiometric amounts of metal nitrates are dissolved in distilled water with the help of magnetic stirrer. Further, a solution of citric acid is added to

the mixed metal solution with molar ratio of nitrates to citric acid is 1:3. This mixed solution is constantly stirred on a hot plate at 50 °C for about 30 minutes. Aqueous ammonia solution is then added drop by drop under constant stirring in order to adjust the pH value to about 7. Further, the mixed solution is continuously heated at 120°C with uniform stirring until a viscous gel is obtained. When all water molecules are removed from the mixture, the gel automatically ignite to give black fluffy powder. The powder materials are ground in a gate mortar for about 30 minutes. To obtain a pure phase compound, the obtained powder is heated at 700 °C for 8 hours in air with a heating and cooling rate of 5 and 2 °C/min, respectively. Finally, the obtained samples are ground in agate mortar for about 30 minutes to obtain the required powder materials.

## 2.2. Characterization

The crystalline structures of both samples in the powder form are analyzed by Philips X-ray diffractometer, using the Cu Kα radiation with λ equal to 1.54178 Å. The X-ray diffraction spectrum is obtained by scanning over a 2θ angular range from 10 to 90 degrees. FT-IR spectroscopy measurements are conducted by Shimadzu FT-IR-8900 instrument in transmittance method with potassium Bromide (KBr) as IR window in the wave number region of 425 to 1000 cm$^{-1}$. The electrical and dielectric properties of electrodes are performed by Phase Sensitive Multimeter (Model: PSM 1700, UK) at room temperature in the frequency range from 20 Hz to 1 MHz.

## 3. RESULTS AND DISCUSSIONS

### 3.1. X-ray diffraction analysis

The x-ray powder diffraction patterns of $LiMn_{1.92}Co_{0.05}Cr_{0.03}O_4$ and $LiMn_{1.9}Co_{0.05}Cr_{0.05}O$ materials are shown in Fig. 1. As it can be seen from the figure, the well-defined reflection peaks include ten lattice planes at (111), (311), (222), (400), (331), (511), (440), (531), (533)and (622) which are indexed to the cubic structure of spinel $LiMn_2O_4$ with a space group Fd$\bar{3}$m which is in line with Joint Committee on Powder Diffraction Standards (JCPDS) card are obtained. All peaks appeared in the XRD patterns are very sharp and well-defined, indicating a high crystalline of the powder materials. Further, no additional impurity peaks are detected. This indicates that partial substitution of $Co^{3+}$and $Cr^{3+}$ for $Mn^{3+}$ does not change the basic structure of $LiMn_2O_4$. However, as compared the XRD of the two samples, the diffraction peaks of $LiMn_{1.9}Co_{0.05}Cr_{0.05}O_4$ sample is shifted slightly towards higher angles. This indicates the fact that the substitution of higher concentration of $Cr^{3+}$ ions has led to the decrease in the crystal size of $LiMn_2O_4$.
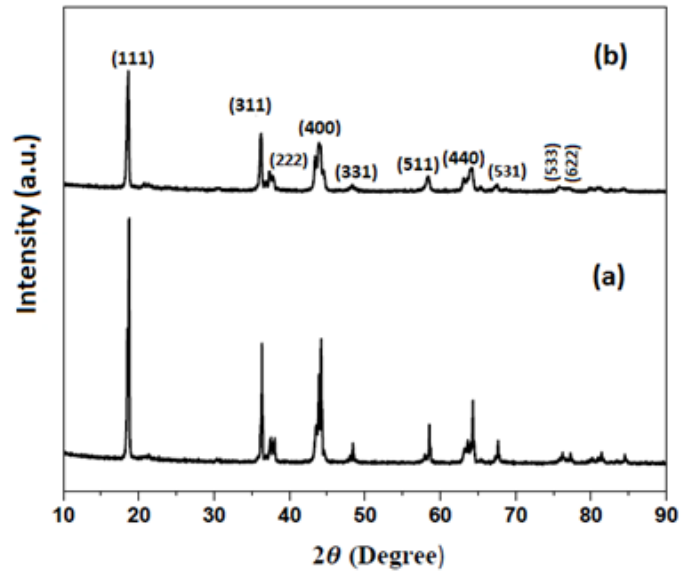


**Figure-1:** X-ray diffraction patterns of (a) $LiMn_{1.92}Co_{0.05}Cr_{0.03}O_4$ and (b) $LiMn_{1.9}Co_{0.05}Cr_{0.05}O_4$.

In order to evaluate the influence of partial substitution of $Co^{3+}$ and $Cr^{3+}$ for $Mn^{3+}$on the structural parameters, the lattice parameter, a, unite cell volume, V, and crystal sizes, L, of both materials are calculated by the relation;

$$a = d\sqrt{h^2 + k^2 + l^2} \qquad (1)$$

$$V = a^3 \qquad (2)$$

$$L = \frac{0.9\lambda}{\beta \cos \theta} \qquad (3)$$

where (h k l) are the Miller indices, d is the inter-planar spacing, λ is the wavelength of Co Kα radiation, β is the full width at half maximum (FWHM) of the diffraction peak and θ is the diffraction angle of the strongest characteristic peak.

The calculated lattice parameters, unite cell volumes and crystal sizes of $Co^{3+}$and $Cr^3$ substituted samples are slightly lower than when compared with the pure $LiMn_2O_4$ (lattice parameter 8.2422 Å) [2]. This effect may be associated with the ionic radius of substituted $Co^{3+}(0.545$ Å$)$ [11] and $Cr^{3+}(0.615$Å$)$ [12] are smaller than the ionic radius of $Mn^{3+}(0.645$Å$)$ [11]. The decrease in cell volume may increase the stability of the spinel structure during the insertion and de insertion of lithium ion. Finally, the variation of lattice parameters of the synthesized spinels and shift of the diffractions line towards larger angles, suggest the effective replacement of $Co^{3+}$ and $Cr^{3+}$ for $Mn^{3+}$in the lattice of the samples.

**Table-1:** Lattice constants, unite cell volumes, and crystal sizes of both sample.

| Samples | Lattice Constant (Å) | Unite Cell Volume (Å)³ | Crystal Size from (111) (nm) |
|---|---|---|---|
| $LiMn_{1.92}Co_{0.05}Cr_{0.03}O_4$ | 8.188 | 548.95 | 58.6 |
| $LiMn_{1.9}Co_{0.05}Cr_{0.05}O_4$ | 8.181 | 547.54 | 57.25 |

## 3.2. FT-IR analysis

In spinel $LiMn_2O_4$ cathode material, the metal cations are situated in two different sub-lattices namely tetrahedral and octahedral sites. The manganese ions exist in two oxidation states, i.e. a trivalent state ($Mn^{3+}$) as well as a tetravalent state ($Mn^{4+}$) in the form of $MnO_6$ ($Mn^{3+}O_6$ and $Mn^{4+}O_6$) groups. The IR spectra of $LiMn_{1.92}Co_{0.05}Cr_{0.03}O_4$ and $LiMn_{1.9}Co_{0.05}Cr_{0.05}O_4$ powders are shown in Fig. 2. Two distinct strong absorption bands which are responsible for the formation of both materials are observed in each spectrum at different wavelength regions. The peaks appeared at higher wave number regions of 619.23 and 620.38 $cm^{-1}$ for (x= 0.03 and 0.05) may be attributed to $M^{3+}$-O (M = Mn, Co, Cr) stretching vibration of $MnO_6$ groups. Whereas, bands at 518.25 and 520.55 $cm^{-1}$ may be associated with the stretching modes of $Mn^{4+}$-O bands at the octahedral sites as reported by Ohzuku et al. [13].
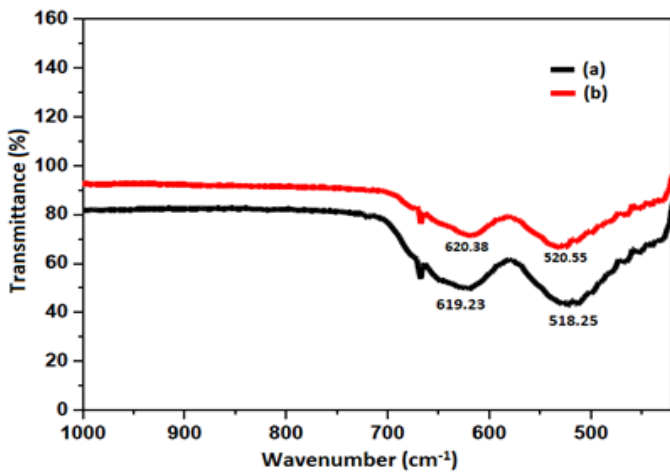


**Figure-2:** FT-IR spectra of (a) $LiMn_{1.92}Co_{0.05}Cr_{0.03}O_4$ and b) $LiMn_{1.9}Co_{0.05}Cr_{0.05}O_4$.

It can be also observed that, the peaks of $LiMn_{1.9}Co_{0.05}Cr_{0.05}O_4$ are shifted slightly towards the higher wave number region. This indicates that the substitution of higher amount of $Cr^{3+}$ for $Mn^{3+}$ (x = 0.05) strengths the Mn–O bonds. This result is in good agreement with the smaller lattice parameter and unit cell volume calculated from the XRD patterns.

## 3.3. Electrical and dielectric properties study

The Nyquist plots of $LiMn_{1.95-x}Co_{0.05}Cr_xO_4$ (where x = 0.03, 0.05) samples measured at room temperature in the frequency range from 1Hz to 1MHz are shown in Fig. 3. It is clearly observed that both spectra are composed of a depressed semicircle in the high frequency and an inclined straight line in the low frequency regions. In this case second semi-circle is not observed, indicating that the grain boundary effect or resistance is negligibly in both samples. Further, the depressed semicircles correspond to the bulk conduction of the materials related to the parallel combination of a bulk resistor and a frequency dependent capacitor. In this case the conductivity is mixed electronic and ionic in character. However, the straight lines at low frequency are due to the electrode polarization (between the sample and silver electrode) as a result of migration of ions at low frequency. It is also observed that the intercept of semicircular arc with real axis is found to decrease for $LiMn_{1.92}Co_{0.05}Cr_{0.03}O_4$ electrode. This indicates that the more electronic conductivity nature of the electrode.
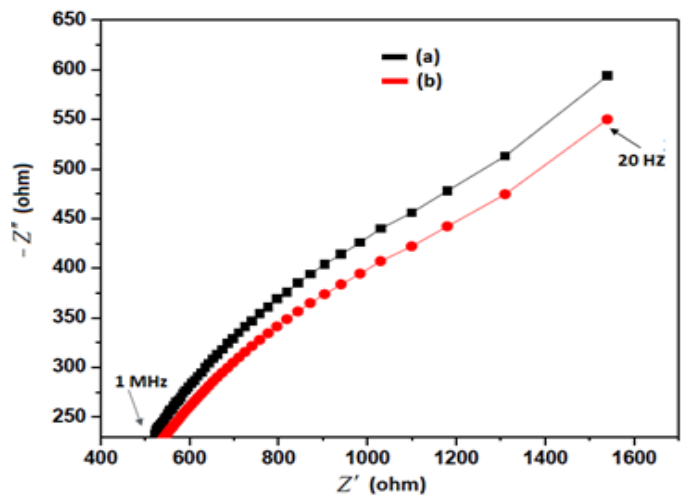


**Figure-3.** Nyquist diagram for (a) $LiMn_{1.92}Co_{0.05}Cr_{0.03}O_4$ and (b) $LiMn_{1.9}Co_{0.05}Cr_{0.05}O_4$.

The low frequency intercept made by the semicircle on the real impedance axis can be used to determine the dc resistance or bulk resistance $R_b$, which is used to calculate the dc conductivity of the materials. The dc conductivity of each sample is calculated using Equation (4) from the measured bulk resistance ($R_b$), area (A) and thickness (L) of the pellet.

$$\sigma_{dc} = \frac{L}{R_b A} \qquad (4)$$

The calculated conductivity results are compared in Table 2. The obtained results of both samples are found to be dependent on the concentration of the substituted Cr ions. At room temperature, the electrical conductivity values are found

to be 8.67 x 10⁻⁵ S.cm⁻¹ for LiMn$_{1.92}$Co$_{0.05}$Cr$_{0.03}$O$_4$ and 7.88 x 10⁻⁵ S.cm⁻¹ and LiMn$_{1.9}$Co$_{0.05}$Cr$_{0.05}$O$_4$ for samples, respectively. G. Singh [14] reported that the electrical conductivity of LiCr$_x$Mn$_{2-x}$O$_4$ samples at room temperature in various compositions (from x = 0.1 to 0.5) is from 6.61 to 1.57 10⁻⁵ S/cm. We feel that the results obtained for the investigated samples are compatible. From this we can suggest that both materials may provide good specific capacity results. On the other hand, the obtained results are found to be in the range of the electrical conductivity of semiconductor (10⁻⁷ to 10³ S/cm), indicating the semiconductor behavior of the samples.

**Table-2.** The conductivity and resistance of both samples.

| Sample | Bulk Resistance R$_b$ (Ω) | Conductivity (S/cm) |
|---|---|---|
| LiMn$_{1.92}$Co$_{0.05}$Cr$_{0.03}$O$_4$ | 1540 | 8.67 x 10⁻⁵ |
| LiMn$_{1.9}$Co$_{0.05}$Cr$_{0.05}$O$_4$ | 1665.3 | 7.88 x 10⁻⁵ |

To investigate the influence of frequency on the conductivity as well the dielectric constant of the synthesized materials, the frequency dependence ac conductivity $\sigma_{ac}$ and the real part of dielectric constant $\varepsilon'$ are calculated using Equations (5) and (6).The comparison of $\sigma_{ac}$ as a function of frequency at room temperature for LiMn$_{1.92}$Co$_{0.05}$Cr$_{0.03}$O$_4$ andLiMn$_{1.9}$Co$_{0.05}$Cr$_{0.05}$O$_4$ materials synthesized by sol-gel method at a temperature of 700°C in air is shown in Fig. 4.

$$\sigma_{ac} = 2\pi f \varepsilon_0 \varepsilon' \tan\delta \qquad (5)$$
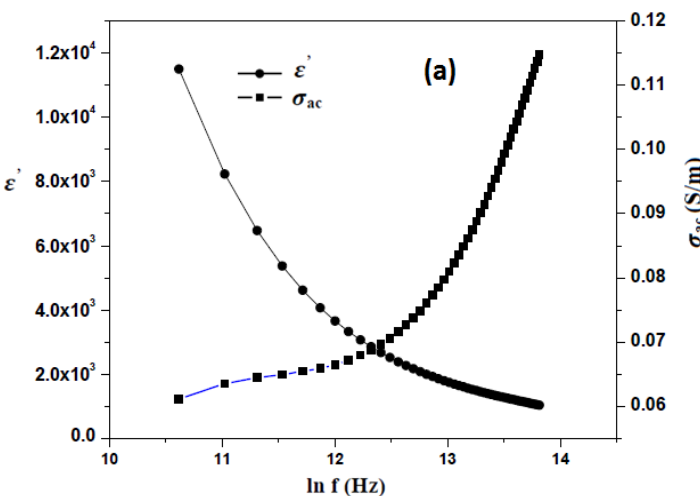
$$\varepsilon' = \frac{CL}{\varepsilon_0 A} \qquad (6)$$

Where f is the frequency, $\varepsilon_0$ is the permittivity of the free spaces, $\tan\delta$ is dielectric loss tangent and C is the capacitance.

From ac conductivity, it can be observed that the plots exhibit two different regions associated with different phenomena. The first one is the low frequency region which describes the electrode–electrolyte interface phenomena, corresponding to frequency independent conductivity (dc conductivity). The second one is the high frequency region in which the conductivity increases rapidly and reaches the highest value at 1 MHz, corresponding to frequency dependent conductivity (ac conductivity). In the high frequency region, the ionic conductivity increases with increasing frequency which is a characteristic of hopping process, indicating correlated forward–backward motions between M³⁺ (M = Mn, Co and Cr) and Mn⁴⁺ ions.

For the case of dielectric constant $\varepsilon'$, it is clear that the value of $\varepsilon'$ decreases dramatically with increasing frequency. The higher values of dielectric constant at lower frequencies can be due to pile-up of charges at the interfaces between the sample and the electrodes. At higher frequencies, the periodic reversal of the electric field with time occurs so fast that there is no excess ion diffusion in the direction of the field, which means that the dipoles in the sample cannot reorient themselves fast enough to respond to the applied electric field. However, at lower frequency region, the dipoles get sufficient time to orient themselves completely along the direction of the field, resulting in larger values of $\varepsilon'$ of the samples.
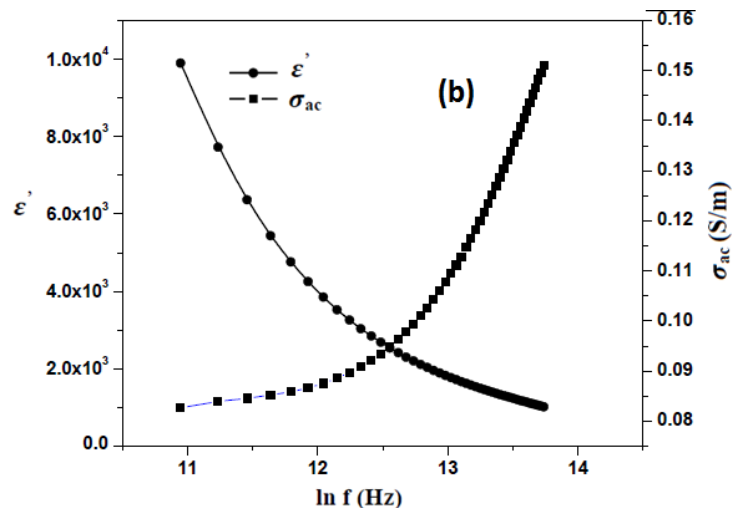


**Figure-4**. Variation of ac conductivity and dielectric constant with frequency at room temperature for (a) LiMn$_{1.92}$Co$_{0.05}$Cr$_{0.03}$O$_4$ and (b) LiMn$_{1.9}$C$_{0.05}$Cr$_{0.05}$O$_4$ samples.
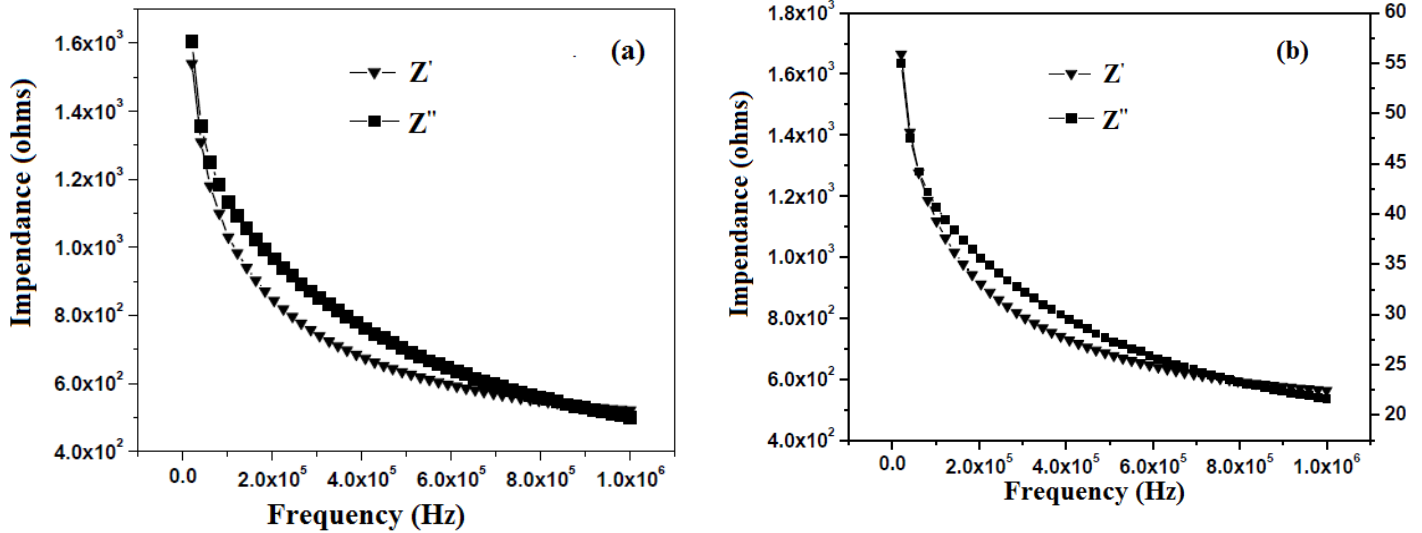
**Figure-5:** Variation of real (Z′) and imaginary ($Z''$) part of impedance for (a) $LiMn_{1.92}Co_{0.05}Cr_{0.03}O_4$ and (b)$LiMn_{1.9}Co_{0.05}Cr_{0.05}O_4$ cathode materials.

Fig. 5 shows the variation of Z′ and $Z''$ part of impedance as a function of frequency at room temperature for $LiMn_{1.92}Co_{0.05}Cr_{0.03}O_4$ and $LiMn_{1.9}Co_{0.05}Cr_{0.05}O_4$ electrodes. From the Fig. 5 (a) and (b), it is observed that the magnitude of Z′ and $Z''$ decreases as the frequency gradually increases, indicating an increase in conductivity of both electrodes due to hopping of electrons. The decreasing values of Z′ and $Z''$ means that the loss in resistive property of the samples. Such a behavior is expected due to the presence of space charge polarization in both materials

## 4. CONCLUSIONS

Using nitrate salts and citric acid as chelating agent, uniform powder $LiMn_{1.95-x}Co_{0.05}Cr_xO_4$ (x=0.03, 0.05) materials are synthesized successfully by sol-gel combustion method. XRD analysis reveals that Cr and Co ions substitution into $LiMn_2O_4$ leads to a decrease in its lattice parameter, unit cell volume and crystal size. This is also supported by the shifting of IR bands towards higher wavelengths. From the XRD analysis, it is also observed that the lattice parameter, the unit cell volume and the crystal size of Co and Cr ions substituted samples decrease with the increase of Cr content to x = 0.05 in $LiMn_{1.95-x}Co_{0.05}Cr_xO_4$. From the frequency dependent plot of ac conductivity, the normal behaviors of the materials are observed. Two distinct regions (the dc and ac conductivities) are identified. The room temperature electrical conductivity values are found to be 8.67 x $10^{-5}$ S.cm$^{-1}$ and 7.88 x $10^{-5}$ S.cm$^{-1}$ for $LiMn_{1.92}Co_{0.05}Cr_{0.03}O_4$ and $LiMn_{1.9}Co_{0.05}Cr_{0.05}O_4$ for samples, respectively.

## REFERENCES

[1] Zhang N, Tang Z , Qing-Hua H, and Xing-He L. Synthesis and characterization of multidoped lithium manganese oxide spinel $LiCo_{0.02}La_{0.01}Mn_{1.97}O_{3.98}Cl_{0.02}$. Trans Nonferrous Met Soc China, vol. 16, 2006, pp. 266-289.

[2] Shen C H, Liu R S, Jang L-Y, Lee J F, and Chen J M. Local Structure and Electronic States of $Li(Mn_{2-x}Co_x)O_4$ Studied by X-ray Absorption Spectroscopy. J. Chinines Chem Soc, vol. 49, 2002, pp. 841-850.

[3] Whittingham C M. Lithium Batteries and Cathode Materials. Chem Rev, vol. 104, 2004, pp. 4271–4301.

[4] Tobishima, Takei K, Sakurai Y, and Yamaki J. Lithium ion cell safety. J Power Sources, vol. 90, 2000, pp. 188–195.

[5] Li L, Ge J, Chen R, Wua F, Chen S, and Zhang X, Environmental friendly leaching reagent for cobalt and lithium recovery from spent lithium-ion batteries. Waste Manag, vol. 30, 2010, pp. 2615-2621.

[6] Hossain S, Seleh Y, and Loutfy R. Carbon-carbon composite as anodes for lithium-ion battery systems. J Power Sources, vol. 96, 2001, pp. 5-13.

[7]  Ryu W H.  Eom J Y, Yin R Z, Han D W,  Kim W K, and Kwon H S. Synergistic effects of various morphologies and Al doping of spinel $LiMn_2O_4$ nanostructures on the electrochemical performance of lithium-rechargeable Batteries. J Mater Chem, vol. 21, 2011, pp. 15337–15342.

[8]  Balaji S, Manichandran T, and Mutharasu D. A comprehensive study on influence of $Nd^{3+}$ substitution on properties of $LiMn_2O_4$. Bull Mater Sci, vol. 35, 2012, pp. 471–480.

[9]  Sathiya M, Annigere, Prakash S, Ramesha K, and Shukla A K. Nitrate-melt synthesized $HT\text{-}LiCoO_2$ as a superior cathode-material for lithium-ion batteries. Mater, vol. 2, 2009, pp. 857-868.

[10]  Toprakci O, Hatice A K, LiwenJi T, and Zhang X. Fabrication and Electrochemical Characteristics of $LiFePO_4$ Powders for Lithium-ion Batteries. KONA Powder and Part J, vol.  28, 2010, pp. 50-73.

[11]  Chunrui X, Yunjiao L, Hu X , Puliang L , Long K , Qianye S,  and Xinlong C. Electrochemical Evaluation of Co-Al Dual-doped $LiMn_2O_4$ Spinels Synthesized Via Hydrothermal Method. Int J Electrochem Sci, vol. 12, 2017, pp. 5185 – 5198.

[12]  Gabal M A, Bayoumy W A, Saeed A, and Al Angari Y M. Structural and electromagnetic of Cr-substituted Ni–Zn ferrites synthesized via Egg-white route. J Molecular Structure, vol. 1097, 2015, pp. 45-51.

[13]  Ohzuku T, Ueda U, Nagayama M, Iwakoshi, and Y, Komori H. Comparative study of $LiCoO_2$, $LiNi_{1/2}Co_{1/2}O_2$  and $LiNiO_2$ for 4 volt secondary lithium cells. Electrochim  Acta. Vol. 38, 1993, pp.1159-1167.

[14]  Singh G, Panwar G, Sil A, and Ghosh S. Synthesis and Characterization of Citric Acid Assisted Cr Doped Lithium Manganese Oxide Spinel. Ceramics – Silikáty, vol. 53, 2009, pp. 260-267.